American Mineralogist, Volume 83, pages 68–74, 1998

Equation of state of brucite: Single-crystal Brillouin spectroscopy study and polycrystalline pressure-volume-temperature measurement

X. Xia, D.J. Weidner, and H. Zhao

Center for High Pressure Research and Department of Geosciences, State University of New York at Stony Brook, Stony Brook, New York 11794-2100, U.S.A.

Abstract

Acoustic velocities of brucite were measured at room pressure in over 48 directions from Brillouin spectroscopy using a natural sample. These data are supplemented with volume measurements as a function of pressure and temperature that range from ambient conditions to 11 GPa and 873 K using synchrotron X-ray radiation at the National Synchrotron Light Source (NSLS) in a cubic-anvil apparatus (SAM-85) with a synthetic polycrystalline sample. The diffraction patterns are collected during cooling cycles to minimize the effect of deviatoric stress on the measurements. These data yield internally consistent thermoelastic parameters defining the equation of state of brucite along with the single-crystal elastic moduli. The Brillouin spectroscopy measurements are best fit with the following elastic model: C_{11} = 156.7(8), C_{33} = 46.3(8), C_{44} = 21.7(5), C_{12} = 44.4(10), C_{13} = 12.0(15), and C_{14} = 0.2(8) GPa. The resultant linear compressibilities of the *a* and *c* axes are 3.8(1) × 10^{-3} and 19.6(6) × 10^{-3} (GPa^{-1}), respectively, with the Reuss bound for the bulk modulus, K_R = 36.7(10) GPa and the Hill average, K_H = 46(1) GPa. The unit-cell parameters (*a, c,* and volume) determined from the diffraction measurements were fit with a Birch-Murnaghan equation of state, yielding K_0 = 39.6(14) Gpa, K' = 6.7(7), $(\partial K_T/\partial T)_P$ = −0.0114(16) GPa/K, and α = 5.0(7) × 10^{-5}/K. The bulk modulus and linear compressibilities from X-ray diffraction are in agreement with those from Brillouin spectroscopy. The ratio of linear compressibility of the *a* to *c* axes is about five times at ambient conditions and reduces to almost unity by 10 GPa. The axial thermal expansions reflect a similar pressure dependence. The ambient shear anisotropy (C_{44}/C_{66}) is about 2.5.

Introduction

Brucite provides a particularly useful platform to study the effect of pressure on the manner that H affects physical properties of minerals. The brucite structure consists of layers with octahedrally coordinated Mg, separated by layers containing only H (Fig. 1). The crystal structure of brucite is trigonal and the space group is $P3m1$ (Zigan and Rothbauer 1967). Each O atom in the hexagonally closed-packed layers is bonded with H such that the O-H bond is perpendicular to the layers, with bond length close to 1 Å, while the distance between the layers of octahedra containing Mg is about 2.7 Å (Parise et al. 1994). Thus, thermal expansion and hydrostatic compression of the *a* axis (perpendicular to the layers) is dominated by the stronger of the two layers, whereas expansion and compression of the *c* axis (parallel to the layers) reflects the properties of the weaker layer. Because the linear compressibility and thermal expansion of the *a* axis are similar to MgO, the compressibility and expansion of the *c* axis reflects the interactions of the H and O atoms. Thus a detailed study including single-crystal elastic properties and high-pressure, high-temperature cell dimensions can provide some information for understanding the behavior of brucite at high pressure.

Recently brucite has been studied at high pressure using various techniques, such as powder X-ray diffraction (Fei and Mao 1993), single-crystal X-ray diffraction (Duffy et al. 1995), powder neutron diffraction (Parise et al. 1994; Catti et al. 1995), shock wave compression (Duffy et al. 1991), Raman spectra (Kruger et al. 1989), and theoretically (Sherman 1991; D'Arco et al. 1993). These studies showed that the linear compressibilities of the *a* and *c* axes are different and that the pressure dependence of these compressibilities is very different. Such behavior gives rise to deviatoric stresses under pressure that in turn can increase uncertainties in cell dimensions and indure errors in determinations of equations of state at pressure. Hence it is important to minimize the deviatoric stresses to get good data on bulk modulus. In the first part of this paper, we report the results of a single-crystal Brillouin spectroscopy study using a natural brucite sample. These data are sufficient to define all elastic properties at ambient conditions, including the aggregate bulk modulus and linear compressibilities that are appropriate to hydrostatic pressure conditions. In the second part of this paper, we report results from an X-ray power diffraction study using cubic-anvil apparatus (SAM-85) with in situ synchrotron X-ray along with the

0003–004X/98/0102–0068$05.00

TABLE 1. Acoustic velocities of brucite

	Direction			*V*p			*V*s			*V*s		
	x	*y*	*z*	exp	theor	diff	exp	theor	diff	exp	theor	diff
1	0.8503	−0.5133	−0.1167	8.0184	8.075	−0.0531	3.0352	3.0341	−0.0011	4.8190	4.8349	−0.0159
2	0.6430	−0.6611	−0.3867	7.8508	7.6129	0.2379	3.2508	3.1801	0.0707	4.7257	4.6243	0.1014
3	0.5620	−0.7405	−0.3685	7.6920	7.6586	0.0334	3.1979	3.1664	0.0315	4.6248	4.6479	−0.0231
4	0.4653	−0.8049	−0.3684	7.6913	7.6575	0.0338	3.1548	3.1673	−0.0125	4.6654	4.6508	0.0146
5	0.5887	−0.6304	−0.5060	7.3229	7.2335	0.0894	3.3530	3.2877	0.0653	4.5614	4.4537	0.1077
6	0.3074	−0.7766	−0.5499	—			—			4.3637	4.3876	−0.0239
7	0.1043	−0.7085	−0.6979	—			3.5349	3.4985	0.0364	—		
8	0.8443	−0.5047	−0.1800	7.7882	8.0098	−0.2216	3.0225	3.0543	−0.0318	4.7017	4.8052	−0.1035
9	0.6529	0.0882	−0.7523	6.0847	6.0026	0.0821	3.4761	3.5552	−0.0791	—		
10	0.6573	−0.7058	−0.2643	7.7666	7.8846	−0.1180	3.0852	3.0957	−0.0105	4.6676	4.7490	−0.0814
11	0.7873	−0.6085	−0.0993	7.8536	8.0830	−0.2294	2.9656	3.0299	−0.0643	4.7583	4.8407	−0.0824
12	0.6217	−0.7751	−0.1128	7.7571	8.0732	−0.3161	—			4.6633	4.8373	−0.1740
13	0.4709	−0.8735	−0.1230	7.8403	8.0638	−0.2235	—			4.6969	4.8346	−0.1377
14	0.4425	−0.5525	−0.7063	6.0605	6.2906	−0.2301	3.5131	3.5044	0.0087	—		
15	0.2194	−0.1609	−0.9623	4.4532	4.5383	−0.0851	—			—		
16	−0.0455	0.0430	−0.9980	4.3663	4.4146	−0.0483	3.0275	3.0301	−0.0026	—		
17	−0.5692	0.3084	−0.7621	5.8898	5.9331	−0.0433	3.5395	3.5660	−0.0265	—		
18	−0.9611	0.2055	−0.1847	—			—			4.7381	4.8122	−0.0702
19	−0.7975	0.5760	−0.1795	—			2.9273	3.0568	−0.1295	4.6351	4.8122	−0.1771
20	−0.4473	0.8640	0.2313	—			—			4.5750	4.7777	−0.2027
21	−0.0069	−0.4154	−0.9096	—			3.5318	3.5898	−0.0580	—		
22	−0.6750	−0.0731	−0.7342	6.2914	6.1228	0.1686	3.5093	3.5349	−0.0256	—		
23	−0.2860	−0.2427	−0.9270	4.7692	4.7466	0.0226	3.5441	3.5531	−0.0090	—		
24	−0.2505	−0.1092	−0.9619	4.5491	4.5397	0.0094	—			3.3428	3.3868	−0.0440
25	−0.3088	−0.2316	−0.9225	—			3.5677	3.5659	0.0018	—		
26	0.0991	0.2167	−0.9712	4.5037	4.4979	0.0058	3.2991	3.3148	−0.0157	—		
27	0.0969	0.3785	−0.9205	4.9842	4.7909	0.1933	—			3.6334	3.5704	0.0630
28	0.5354	0.1664	−0.8281	5.2570	5.4767	−0.2197	—			3.6598	3.6185	0.0413
29	0.8194	−0.5723	−0.0324	8.3537	8.1112	0.2425	3.1207	3.0204	0.1003	5.0932	4.8550	0.2382
30	−0.9995	−0.0190	−0.0255	—			—			5.0259	4.8563	0.1696
31	−0.9826	0.1837	−0.0264	7.9057	8.1115	−0.2058	2.9867	3.0203	−0.0336	4.7366	4.8563	−0.1197
32	−0.9987	0.0310	−0.0414	8.3852	8.1088	0.2764	—			5.0137	4.8550	0.1587
33	−0.9969	−0.0648	−0.0456	8.2854	8.1079	0.1775	—			5.0926	4.8524	0.2384
34	−0.9286	0.3706	−0.0185	8.1319	8.1128	0.0191	—			—		
35	−0.8504	0.5260	−0.0087	8.3261	8.1136	0.2125	—			4.9574	4.8571	0.1003
36	0.0498	−0.0347	0.9982	4.4849	4.4147	0.0702	3.0319	3.0303	0.0016	—		
37	−0.2422	−0.8562	0.4564	—			—			4.6734	5.5307	0.1427
38	−0.3205	−0.9353	−0.1498	—			2.9998	3.0451	−0.0453	4.8344	4.8251	0.0093
39	−0.4819	−0.8653	−0.1380	7.9926	8.0515	−0.0589	—			4.8039	4.8290	−0.0251
40	−0.4896	−0.8611	−0.1373	8.0516	8.0524	−0.0008	—			4.8277	4.8293	−0.0016
41	−0.6268	−0.7696	−0.1219	—			—			4.8530	4.8340	0.0190
42	0.0577	0.3935	−0.9175	4.8389	4.8132	0.0257	3.5476	3.5780	−0.0304	—		
43	−0.2439	0.3083	−0.9195	4.5682	4.7925	−0.2243	—			3.4050	3.3737	0.0313
44	−0.3060	0.1194	−0.9445	4.5558	4.6282	−0.0724	—			3.2396	3.2757	−0.0361
45	−0.1880	0.4933	−0.8493	—			3.7063	3.6269	0.0794	—		
46	−0.3156	−0.9489	0.0007	8.0722	8.1143	−0.0421	4.7888	4.8573	−0.0685	—		
47	−0.4755	−0.8797	0.0020	8.1186	8.1141	0.0045	4.8499	4.8572	−0.0073	—		
48	−0.6218	−0.7832	0.0000	8.0287	8.1144	−0.0857	4.8366	4.8573	−0.0207	—		

Note: x parallel to *a**, *y* parallel to *b**, and *z* parallel to *c*. For details, see Vaughan and Guggenheim 1986.

equation of state methodologies that we developed to minimize deviatoric stresses (Weidner et al. 1992; Wang et al. 1994). The bulk modulus deduced from crystallography agrees very well with the value derived from Brillouin spectroscopy corresponding to hydrostatic stress (the Reuss bound), whereas other reported values approach the Hill or even the Voight value of bulk modulus, indicating that deviatoric stresses are present in these studies.

SINGLE-CRYSTAL BRILLOUIN SPECTROSCOPY

Experimental procedures

The single crystal used in this study is a naturally occuring brucite. It has (001) cleavage and six growth faces, with dimensions of approximately 3 × 6 × 6 mm. Its chemical composition is nearly pure, $Mg(OH)_2$. Trace element abundances determined by X-ray fluorescence are 9 ± 10 ppm Fe; <20 ± 30 ppm Ca; 14 ± 10 ppm V; 90 ± 10 ppm Mn; 7 ± 5 ppm Zn; 7 ± 5 ppm As. The refractive indices were determined using the immersion fluid method with 5145 Å light as W = 1.57(1) and E = 1.59(1). The unit-cell parameters of the sample were determined using four-circle X-ray diffractometer, yielding of a = 3.14(1) Å, c = 4.76(1) Å, and cell volume = 40.8(1) $Å^3$, consistent with previous results for brucite (Fei and Mao 1993; Duffy et al. 1995; Catti et al. 1995). The density used in this study is 2.38(1) (g/cm^3) was calculated from the X-ray data. The sample was mounted on a goniometer head and the orientation matrix was determined using a four-circle X-ray diffractometer. Then it

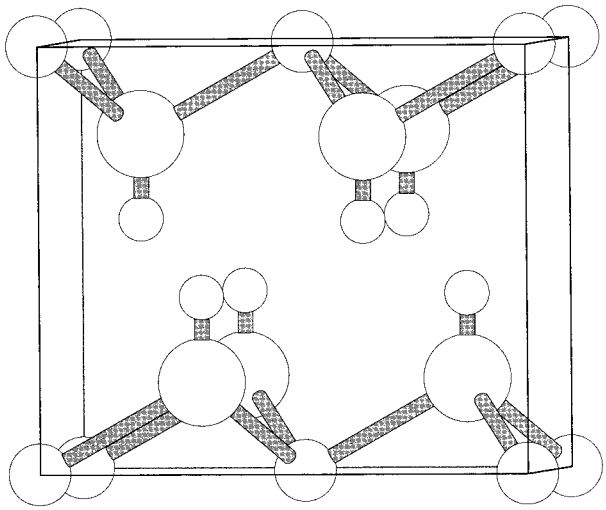

FIGURE 1. The structure of brucite. Big ball represents O, medium ball represents Mg, and small ball represents H.

was transferred to the three-circle Eulerian cradle with its orientation preserved and immersed in a liquid with a nearly matching refractive index. The experimental procedure was discussed elsewhere (Vaughan 1979). Brillouin spectra were measured in over 48 directions to constrain the six elastic moduli. Table 1 compares the observed velocities (exp) with those predicted by the best-fit elastic moduli model (theor) with the difference between these indicated by diff.

Results and discussion

The six elastic constants for trigonal brucite (Table 2) exhibit a striking anisotropy. The elastic constant C_{11} is about four times greater than C_{33}. This pattern is related to the layered structure in which the chemical bonding between the layers and along the layers is different. From other brucite-like minerals (e.g., CdI_2 structure) and other layered minerals such as muscovite, large differences also exist between the *c* and *a* axes in (Table 2).

The elastic moduli are recast as linear compressibilities in Table 3. From our work, the linear compressibility of the *c* axis of brucite is about five times greater than that of the *a* axis. This difference is consistent with the results from Fei and Mao (1993) and Duffy et al. (1995). In this study, the linear compressibility of the *a* axis, (3.8×10^{-3} GPa^{-1}), is close to two times that of periclase (2.1×10^{-3} GPa^{-1}, Bass 1995), consistent with the structure of brucite (half of the octahedral sites in its hexagonally closed-packed layers of O are occupied and half are empty).

The shear anisotropy C_{66}/C_{44} is about 2.5, which is lower than the ratio of linear compressibilities. A systematic relationship exists between the ratio of linear compressibilities and the shear anisotropy for several layer minerals (Fig. 2). The shear anisotropy is very high in graphite (Zhao and Spain 1989), low in CdI_2, PbI_2 (Sandercock 1975), and intermediate in brucite.

Because of anisotropy, the calculated Reuss and Voigt bounds for the bulk properties of brucite (Table 4) are different. In experiments where each grain is under hydrostatic pressure, compression studies yield the Reuss bound for the bulk modulus. Experiments in which a polycrystal is under hydrostatic pressure such that the individual grains possess ''welded'' type boundary condi-

TABLE 2. Some elastic constants of brucite and related minerals (GPa)

C_{ij}	$MG(OH)_2$*	SnS_2†	CdI_2†	PbI_2†	$Ca(OH)_2$‡	Muscovite§
11	156.7(8)	14.6	4.31	2.77	99.28	181.0
22	156.7(8)	14.6	4.31	2.77	99.28	178.4
33	46.3(8)	2.72	2.25	2.02	32.6	58.6
44	21.7(5)					
12	44.4(10)					
13	12.0(15)					
14	0.2(8)					

* This work.
† Sandercock 1975.
‡ Holuj et al. 1985.
§ Vaughan and Guggenheim 1986.

TABLE 3. Linear compressibility of brucite (10^{-3} GPa^{-1})

β_c	β_a	β_c/β_a	Reference
13.3	2.5	5	Fei and Mao 1993
12.8	3.3	4	Duffy et al. 1995
17.4	3.2	5	Catti et al. 1995
19.6(6)	3.8(1)	5(0.2)	This work, Brillouin spectroscopy
18.3(15)	4.2(2)	4.4(0.2)	This work, X-ray diffraction

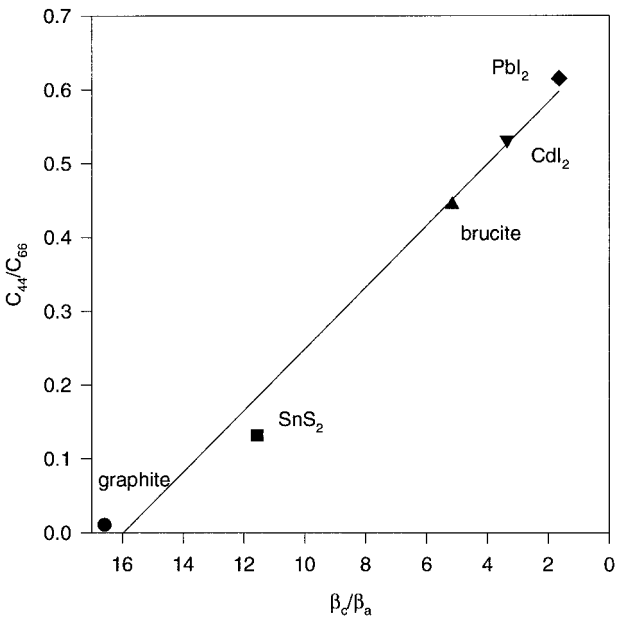

FIGURE 2. The shear anisotropy of brucite and related minerals. ● = graphite (Zhao and Spain 1989); ■ = SnS_2 (Sandercock 1975); ▲ = brucite (this work); ▼ = CdI_2 (Sandercock 1975); ◆ = PbI_2 (Sandercock 1975).

TABLE 4. Calculated elastic moduli and velocities

	Reuss	H-S+	H-S−	Voigt
Bulk modulus (GPa)	36.7	42.6	47.7	55.2
Shear modulus (GPa)	30.4	33.4	35.8	39.3
Longitude velocity (km/s)	5.697	6.054	6.330	6.724
Shear velocity (km/s)	3.574	3.749	3.876	4.065

Note: H-S = Hashin-Shtrikman.

TABLE 5. Bulk modulus of brucite (GPa)

K_0	Method	Reference
54.3	Powder X-ray diffraction	Fei and Mao (1993)
51	Shock compression	Duffy et al. (1991)
47	Powder neutron diffraction	Parise et al. (1994)
42	Single-crystal X-ray diffraction	Duffy et al. (1995)
39	Powder neutron diffraction	Catti et al. (1995)
36.7	Single-crystal Brillouin scattering	This work
39.6	Powder X-ray diffraction	This work

tions exhibit a bulk modulus closer to the average of the Reuss and Voigt bounds. Recent determination of the bulk modulu of brucite are listed in Table 5. We found that data from Fei and Mao (1993) are very high and close to Voigt value and data from Catti et al. (1995) are close to Reuss value. We expect that this large range of experimental bulk moduli reflects the influence of deviatoric stress on the sample.

IN SITU X-RAY DIFFRACTION

Experimental procedure

The powdered sample was synthesized hydrothermally from ultra-high purity MgO with excess deionized, distilled H_2O. These materials were loaded into a Teflon vessel, placed in a oven and held at 200 °C for a week. The solid product was analyzed with X-ray diffraction, which confirmed that it was brucite. No other phases were detected.

Experiments were performed using a cubic anvil apparatus (SAM-85) with the white synchrotron radiation from the superconducting wiggler magnet (X17 beamline) at the Brookhaven National Lab. Diffraction patterns were collected using energy dispersive techniques with a fixed angle ($2\theta = 7.5°$) solid state Ge detector, and collecting time for each diffraction pattern of 200–250 s.

The cell assembly used in this study has been described in detail elsewhere (e.g., Wang et al. 1994). In this experiment, the brucite sample was packed into a boron nitride container of 1 mm diameter and 2 mm length bounded by powdered layers of NaCl on the top and bottom, which served as an internal pressure standard. The temperature was measured by a W-Re24%–W-Re26% thermocouple at the center of the furnace contacting the sample. Pressure was calculated from Decker's equation of state (Decker 1971) using the internal NaCl standard, and the uncertainty in pressure mainly arose because of inconsistencies among different diffraction lines and was less than 0.2 GPa (Weidner et al. 1992; Zhang et al. 1997).

Procedures are discussed in detail elsewhere (Wang et al. 1994). In this experiment, the sample was compressed up to 11 GPa and then heated to about 1000 K, and diffraction patterns were collected at about 100 K intervals during the cooling cycle. It has been our experience that deviatoric stress relaxes upon heating and that data taken on the cooling cycle are relatively free of such complicating effects. Several cooling cycles were performed at

TABLE 6. Cell dimensions of brucite

P (GPa)	*T* (K)	*a* (Å)	*c* (Å)	*V* (Å)
9.24	877	3.064(1)	4.457(1)	36.26(2)
8.95	769	3.063(1)	4.445(1)	36.13(2)
8.97	671	3.061(1)	4.437(1)	36.00(2)
8.68	572	3.060(1)	4.429(1)	35.92(2)
8.50	478	3.058(1)	4.424(1)	35.83(2)
8.40	299	3.054(1)	4.414(1)	35.67(2)
7.75	874	3.080(1)	4.503(1)	37.00(2)
7.55	770	3.079(1)	4.489(1)	36.86(2)
7.53	672	3.075(1)	4.484(1)	36.73(2)
7.23	575	3.075(1)	4.473(1)	36.65(2)
7.11	471	3.073(1)	4.465(1)	36.52(2)
6.79	301	3.068(1)	4.457(1)	36.35(2)
8.71	1040	3.072(1)	4.492(1)	36.73(2)
8.29	873	3.072(1)	4.477(1)	36.61(2)
8.36	772	3.070(1)	4.469(1)	36.49(2)
8.13	674	3.070(1)	4.460(1)	36.40(2)
7.97	522	3.067(1)	4.449(1)	36.26(2)
7.63	415	3.065(1)	4.443(1)	36.17(2)
7.59	300	3.062(1)	4.440(1)	36.06(2)
6.85	872	3.089(1)	4.528(1)	37.43(2)
6.66	773	3.089(1)	4.518(1)	37.29(2)
6.45	670	3.086(1)	4.509(1)	37.18(2)
6.30	573	3.084(1)	4.501(1)	37.09(2)
6.13	471	3.083(1)	4.494(1)	37.01(2)
5.87	301	3.080(1)	4.486(1)	36.87(2)
7.29	869	3.084(1)	4.512(1)	37.16(2)
7.09	769	3.084(1)	4.498(1)	37.05(2)
6.90	671	3.081(1)	4.490(1)	36.91(2)
6.75	574	3.079(1)	4.485(1)	36.84(2)
6.62	474	3.078(1)	4.479(1)	36.77(2)
6.38	301	3.075(1)	4.471(1)	36.61(2)
4.94	875	3.105(1)	4.580(1)	38.26(2)
4.83	769	3.104(1)	4.570(1)	38.13(2)
4.66	671	3.102(1)	4.560(1)	38.01(2)
4.47	573	3.100(1)	4.550(1)	37.88(2)
4.32	471	3.099(1)	4.544(1)	37.80(2)
4.12	301	3.095(1)	4.534(1)	37.63(2)
6.02	874	3.097(1)	4.555(1)	37.84(2)
5.68	773	3.096(1)	4.543(1)	37.71(2)
5.53	673	3.094(1)	4.533(1)	37.60(2)
5.35	573	3.091(1)	4.527(1)	37.47(2)
5.24	473	3.090(1)	4.520(1)	37.39(2)
5.05	301	3.088(1)	4.510(1)	37.25(2)
4.71	877	3.111(1)	4.606(1)	38.62(2)
4.57	770	3.110(1)	4.593(1)	38.47(2)
4.39	672	3.108(1)	4.582(1)	38.34(2)
4.24	573	3.106(1)	4.573(1)	38.21(2)
4.07	471	3.105(1)	4.566(1)	38.13(2)
3.79	301	3.103(1)	4.555(1)	37.97(2)
3.86	774	3.113(1)	4.619(1)	38.88(2)
3.68	674	3.112(1)	4.613(1)	38.70(2)
3.50	573	3.112(1)	4.600(1)	38.66(2)
3.33	473	3.112(1)	4.593(1)	38.51(2)
3.06	301	3.110(1)	4.586(1)	38.41(2)

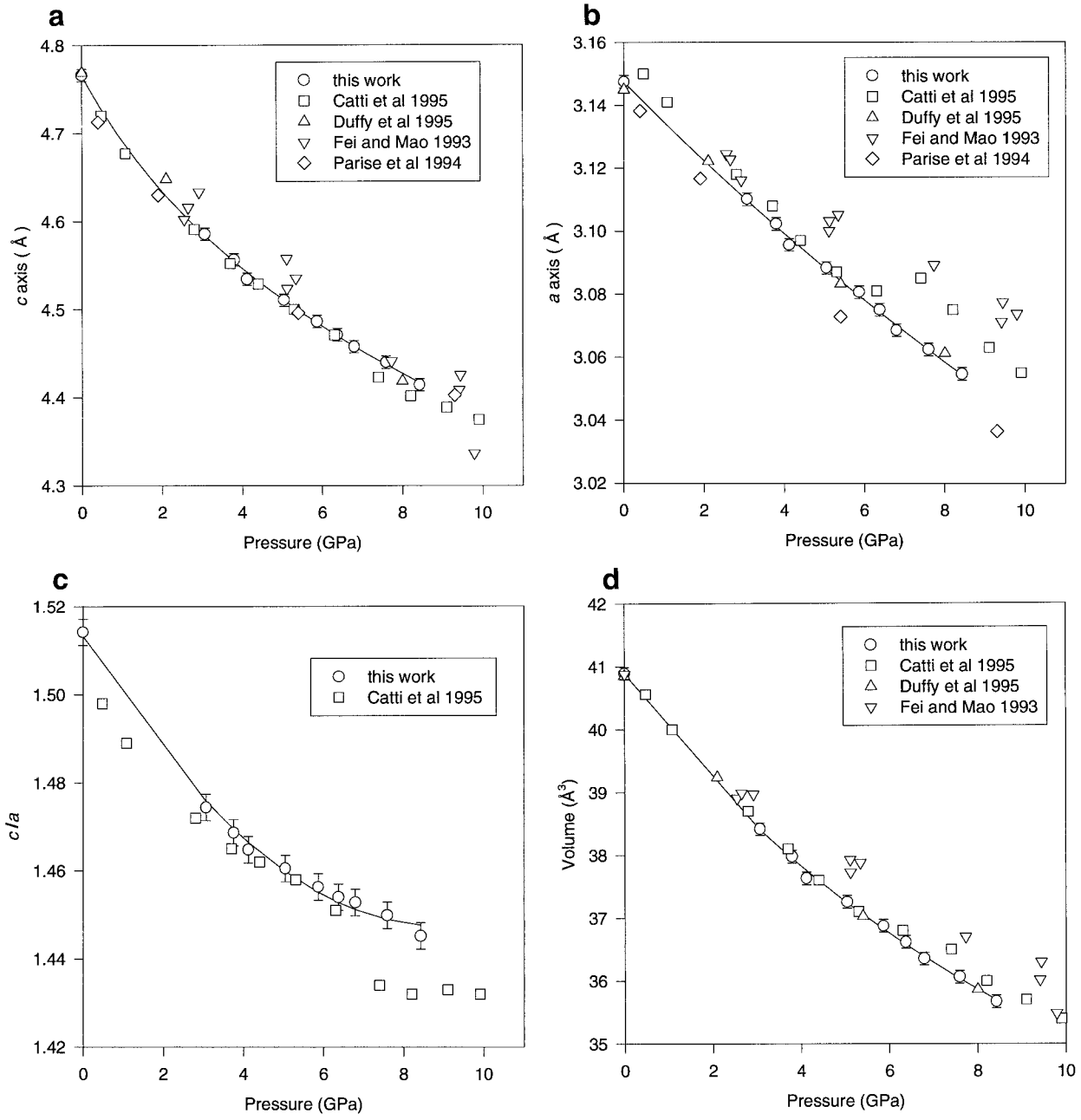

FIGURE 3. The unit-cell parameters as a function of pressure. (**a**) *c* unit-cell length (**b**) *a* unit-cell length (**c**) *c*/*a* ratio, and (**d**) volume. Data at pressures above 10 GPa have been omitted.

different pressures to cover the experimental *P-T* range. Diffraction spectra after the high-pressure experiment appear identical to the starting spectra.

Results and discussion

Room temperature results. Unit-cell parameters *a*, *c*, and volume (Table 6) are shown as a function of pressure at room temperature in Figure 3 and compared to previous results (Duffy et al. 1995; Catti et al. 1995; Parise et al. 1994; Fei and Mao 1993) The pressure dependencies of the unit-cell parameters *a* and *c* clearly differ. Figure 3c illustrates the pressure dependence of the ratio. Catti et al. (1995) reported a discontinuous change in *c*/*a* ratio at pressures of 6 to 7 GPa and room temperature, which they interpreted as a phase transition. As seen in this diagram, we do not observe discontinuity in the *c*/*a* ratio near this pressure and thus do not require a phase transition.

The room-temperature data (Fig. 3) were fit to a Birch-Murnaghan equation of state that has the form:

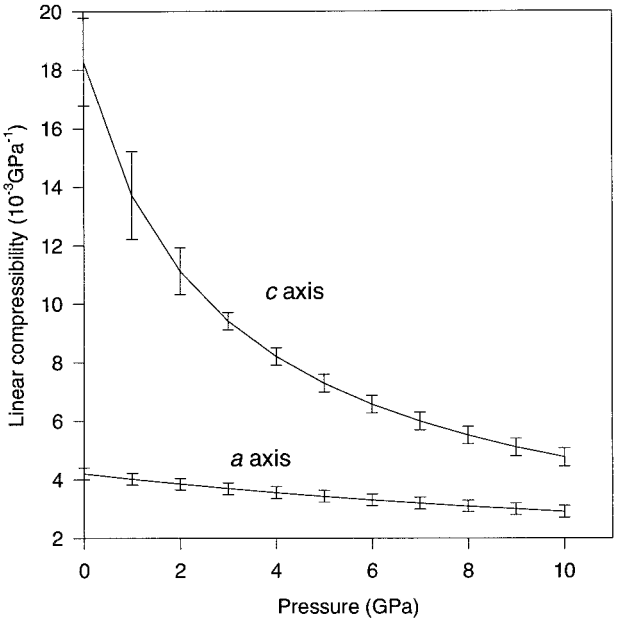

FIGURE 4. The calculated linear compressibilities of brucite as a function of pressure, which is obtained from the derivative of isothermal fitting.

$$P = 3/2K_0[(V_0/V)^{7/3} - (V_0/V)^{5/3}]\cdot\{1 + 3/4(K_0' - 4)\cdot [(V_0/V)^{2/3} - 1]\}, \quad (1)$$

yielding K_0 = 39.6 (14) GPa, K' = 6.7 (7). The bulk modulus is consistent with that obtained from Brillouin spectroscopy (Table 5) and close to results from Catti et al. (1995) and Duffy et al. (1995). Because of the differences in pressure dependence of the cell parameters, *a* and *c*, it is interesting not only to apply an equation of state to volume, but also to the *a* and *c* axes. For this we simply use the parametric form of the Birch-Murnaghan equation of state, but for a^3 and c^3, respectively. The modified equation is

$$P = 3/2K_0[(c_0/c)^7 - (c_0/c)^5]\cdot\{1 + 3/4(K_0' - 4)\cdot [(c_0/c)^2 - 1]\}, \quad (2)$$

yielding K_c = 18.24 (76) GPa, = 6.27 (49), and K_a = 79.1 (23) GPa, = 3.7 (8). A large anisotropy exists between the *a* and *c* axes.

The linear compressibility is given by the derivative of pressure dependence of the unit-cell length, which has the form

$$\beta_1 = -\frac{1}{l}\left(\frac{\partial l}{\partial P}\right)_T \quad (3)$$

where l is the cell parameter *a* or *c*. Using the Birch-Murnaghan equation of state described above, Equation 3 becomes

TABLE 7. Birch-Murnaghan equation-of-state parameters of brucite at high temperature

Method	K_0(GPa)	K_0'(GPa)	$(\partial K_T/\partial T)_P$	$\alpha_0(10^{-5})$	$\alpha_1(10^{-8})$
Volume	38.7(15)	7.0(8)	−0.015(4)	7.3(3)	3.6(13)
c axis	16.9(10)	6.4(7)	−0.008(1)	18.2(3)	−2.7(20)
a axis	80.5(13)	3.4(4)	0.001(3)	3.2(2)	−0.8(9)

$$\beta_1 = -\frac{1}{l}\frac{1}{\left(\frac{\partial P}{\partial l}\right)_T}. \quad (4)$$

The calculated results (Figure 4) demonstrate a large pressure dependence for the *c* axis compressibility, whereas the pressure dependence of *a* axis compressibility is very small. At ambient conditions, the extrapolated linear compressibilities for *c* and *a* axes are (Table 3) close to the results of Brillouin spectroscopy. We expect that the linear compressibility of the *c* axis is underestimated if deviatoric stress is present.

High-temperature Birch-Murnaghan equation of state. The above analysis of volume data along the room temperature isotherm uses only a subset of the data in the *P-T* range of study. It is more reasonable to use all of the data set in fitting, and several approaches are suggested by Jackson and Rigden (1996). In this study, we choose the modified Birch-Murnaghan equation of state with room-pressure parameters replaced by their room pressure-high temperature counterpart (Zhang et al. 1997; Saxena and Zhang 1990). The formulations for those parameters are given by:

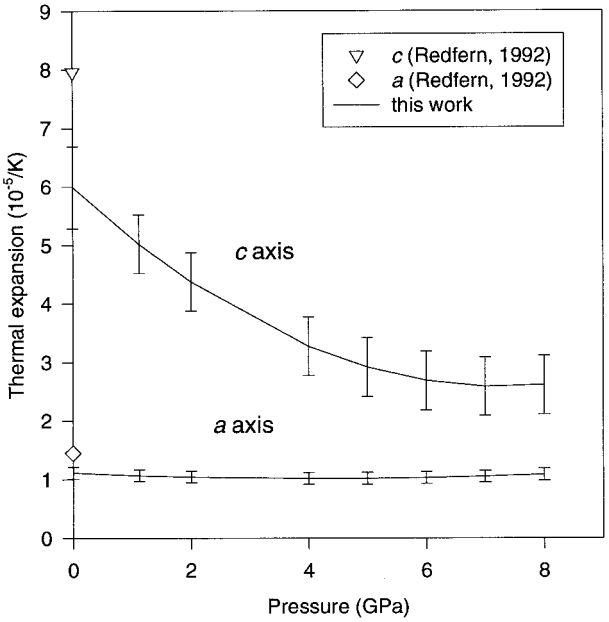

FIGURE 5. The calculated thermal expansion as a function of pressure. The thermal expansions are calculated at isobaric condition with interpolated data from isothermal fitting.

$$K_T = K_0 + (\partial K_T/\partial T)_P(T - 300) \quad (5)$$

$$K_T' = K_0' + (\partial K_T/\partial T)_P(T - 300) \quad (6)$$

$$V_T = V_0\left[\exp\left(\int_{300}^{T} \alpha(T)\, \mathrm{d}T\right)\right] \quad (7)$$

where $\alpha(T)$ is given by:

$$\alpha(T) = \alpha_0 + \alpha_1 T. \quad (8)$$

Room-pressure, high-temperature cell parameter data can help constrain the thermoelastic properties of brucite. We supplemented our *P-V-T* data with the room pressure data of Fei and Mao (1993). We did not use the data of Redfern and Wood (1992) because their data appear to have a small but systematic offset of volume relative to both our data and that of others (Fei and Mao 1993; Duffy et al. 1995; Catti et al. 1995). With this enhanced data set, the calculated coefficients are shown in Table 7 for volume as well as a^3 and c^3.

Axial thermal expansions can be calculated at certain pressure with the parameters shown in Table 7 and results are shown in Figure 5 as a function of pressure. The *c* axis thermal expansion decreases by a factor of two, whereas the *a* axis thermal expansion is nearly pressure independent. At zero pressure, the thermal expansions for the *a* and *c* axis are 6.0(10), and 1.1(2) ($\times 10^{-5}$/K), respectively, which are close to the values of 7.96 and 1.45 ($\times 10^{-5}$/K) from Redfern and Wood (1992).

Acknowledgments

We are grateful to Paul Northrup for providing a sample of brucite for Brillouin spectroscopy and X-ray fluorescence data, M. Kunz for X-ray oriented matrix measurement, Y. Wu for helping SAM85 experiment at NSLS, and to J.B. Parise for helpful discussions. This work is supported by the National Science Foundation through Center for High Pressure Research (EAR-8920239) and partially by grants EAR-9506483 and EAR-9526634. This is MPI publication No. 192.

References cited

Bass, J.D. (1995) Elasticity of minerals, glasses and melts. Mineral Physics and Crystallography, 2, 45–63.

Catti, M., Ferraris, G., Hull, S., and Pavese, A. (1995) Static compression and H disorder in $Mg(OH)_2$ to 11 GPa: A powder neutron diffraction study. Physics and Chemistry of Minerals, 22, 200–206.

D'Arco, P., Causa, M., Roetti, C., and Silvi, B. (1993) Periodic Hartree-Fock study of a weakly bonded layer structure; brucite $Mg(OH)_2$. Physical Review, B47, 3522–3529.

Decker, D.L. (1971) High-pressure equation of state for NaCl, KCl and CsCl. Journal of Applied Physics, 42, 3239–3244.

Duffy, T.S., Ahrens, T.J., and Lange, M.A. (1991) The shock wave equation of state of brucite $Mg(OH)_2$. Journal of Geophysical Research, 96, 14319–14330.

Duffy, T.S., Shu, J., Mao, H.K., and Hemley, R.J. (1995) Single-crystal X-ray diffraction of brucite to 14 GPa. Physics and Chemistry of Minerals, 22, 277–281.

Fei, Y. and Mao, H.K. (1993) Static compression of $Mg(OH)_2$ to 78 GPa at high temperature and constraints on the equation of state of fluid H_2O. Journal of Geophysical Research, 98, 875–11884.

Holuj, F., Drozdowski, M., and Czajkowski, M. (1985) Brillouin spectrum of $Ca(OH)_2$. Solid State Communications, 56, 1019–1021.

Jackson, I. and Ridgen, S. (1996) Analysis of P-V-T data: Constraints on the thermoelastic properties of high pressure minerals. Physics of the Earth and Planetary Interior, 96, 85–112.

Kruger, M., Williams, Q., and Jeanloz, R. (1989) Vibrational spectra of $Mg(OH)_2$ and $Ca(OH)_2$ under pressure. Journal of Chemical Physics, 91, 5910–5915.

Parise, J.B., Leinenweber, K., Weidner, D.J., Tan, K., and Von Dreele, R.B. (1994) Pressure-induced H bonding: Neutron diffraction study of brucite, $Mg(OD)_2$ to 9.3 GPa. American Mineralogist, 79, 193–196.

Redfern, S.A.T. and Wood, B.J. (1992) Thermal expansion of brucite, $Mg(OH)_2$. American Mineralogist, 77, 1129–1132.

Sandercock, J. (1975) Some recent applications of Brillouin scattering in solid state physics. Festkorperprobleme, 15, 183–195.

Saxena, S.K. and Zhang, J. (1990) Thermal chemical and pressure-volume-temperature systematics of data on solids, examples: Tungsten and MgO. Physics and Chemistry of Minerals, 17, 45–51.

Sherman, D.M. (1991) Hartree-Fock band structure, equation of state, and pressure-induced hydrogen bonding in brucite, $Mg(OH)_2$. American Mineralogist, 76, 1769–1772.

Vaughan, M.T. (1979) Elasticity and crystal structure in aluminosilicates and pyroxenes. Ph.D. dissertation. State University of New York at Stony Brook, Stony Brook.

Vaughan, M.T. and Guggenheim, S. (1986) Elasticity of muscovite and its relationship to crystal structure. Journal of Geophysical Research, 91, 4657–4664.

Wang, Y., Weidner, D.J., Liebermann, R.C., and Zhao, Y. (1994) Thermal equation of state of (Mg, Fe)SiO_3 perovskite and constraints on composition of the lower mantle. Physics of the Earth and Planetary Interiors, 83, 13–40.

Weidner, D.J., Vaughan, M.T., Ko, J., Wang, Y., Liu, X., Yeganeh-haeri, A., Pacalo, R.E., and Zhao, Y. (1992) Characterization of stress, pressure, and temperature in SAM85, a DIA type high pressure apparatus. American Geophysical Union, Geophysics Monograph Series, 67, 13–17.

Zhang, J., Martinez, I., Guyot, F., Gillet, P., and Saxena, S.K. (1997) X-ray diffraction study of magnesite at high pressure and high temperature. Physics and Chemistry of Minerals, in press.

Zhao, Y. and Spain, I.L. (1989) X-ray diffraction data for graphite to 20 GPa. Physical Review, B40, 993–997.

Zigan, F. and Rothbauer, R. (1967) Neutronenbeugungsmessungen am brucit. Neues Jahrbuch für Mineralogie Monatsheft, 137–143.

Manuscript received December 4, 1996
Manuscript accepted September 2, 1997